Biophysical Journal
Article

Biophysical Society

Metastatic State of Cancer Cells May Be Indicated by Adhesion Strength

Alexander Fuhrmann,[1] Afsheen Banisadr,[2] Pranjali Beri,[1] Thea D. Tlsty,[3] and Adam J. Engler[1,2,4,*]
[1]Department of Bioengineering and [2]Biomedical Sciences Program, University of California, San Diego, La Jolla, California; [3]Department of Pathology, University of California, San Francisco, San Francisco, California; and [4]Sanford Consortium for Regenerative Medicine, La Jolla, California

ABSTRACT Cancer cells within a tumor are heterogeneous and only a small fraction are able to form secondary tumors. Universal biological markers that clearly identify potentially metastatic cells are limited, which complicates isolation and further study. However, using physical rather than biological characteristics, we have identified Mg^{2+}- and Ca^{2+}-mediated differences in adhesion strength between metastatic and nonmetastatic mammary epithelial cell lines, which occur over concentration ranges similar to those found in tumor stroma. Metastatic cells exhibit remarkable heterogeneity in their adhesion strength under stromal-like conditions, unlike their nonmetastatic counterparts, which exhibit Mg^{2+}- and Ca^{2+}-insensitive adhesion. This heterogeneity is the result of increased sensitivity to Mg^{2+}- and Ca^{2+}-mediated focal adhesion disassembly in metastatic cells, rather than changes in integrin expression or focal adhesion phosphorylation. Strongly adherent metastatic cells exhibit less migratory behavior, similar to nonmetastatic cell lines but contrary to the unselected metastatic cell population. Adhesion strength heterogeneity was observed across multiple cancer cell lines as well as isogenically, suggesting that adhesion strength may serve as a general marker of metastatic cells.

INTRODUCTION

Cancer cell dissemination is a highly coordinated process in which a cell detaches and migrates away from the primary tumor to form a secondary metastatic site (1). However, only a small subset of cancer cells from a tumor or even from a cancer cell line are capable of causing secondary tumors in vivo (2). Successful dissemination requires collagen fiber deposition, alignment, and cross-linking in the adjacent stromal matrix (3,4) to create tracks on which cells migrate. However, this will only occur in cells with labile adhesions (5). Focal adhesion (FA) turnover permits the migration required of invasive cancer cells (6), which tend to have more dynamic FAs than noninvasive cancer cells (7,8). Due to the lack of a consistent set of biomarkers that predict metastatic potential across solid tumors (9), a systematic quantification of adhesion strength could result in a unique biophysical metric to identify highly metastatic cells within a broader tumor cell population. Furthermore, a quantification of tumor cell adhesion strength could serve as a predictor of the metastatic potential of a solid tumor.

Population-based adhesion assays, e.g., the spinning-disk shear assay (10), can monitor FAs by measuring adhesion strength. Specifically, by analyzing the magnitude of shear needed to detach 75% of the cell population (denoted by τ_{25}), we are able to quantify the adhesion strength of a cell population and correlate it with FA assembly. In addition, the spinning-disk shear assay can capture adhesion heterogeneity within a population (11). For example, by plotting a log shear stress versus linear cell density profile, we are able to analyze the logarithmic slope for the resulting sigmoidal curve. From these data, we are able to determine the attachment heterogeneity of a cell type in a variety of conditions. In contrast, single-cell, single-shear, and wash assays cannot quantify these values (8,12–16). Although some studies have shown a correlation between changes in adhesion and secondary tumor development (14–16), substantial phenotypic heterogeneity can exist even within a single cancer cell line (17). Thus, understanding the adhesive heterogeneity within an invasive population may improve our ability to physically monitor cancer cells and predict invasive behavior. Population-based adhesion assays also provide a reductionist niche for determining sensitivity to culture conditions (e.g., cation concentration and matrix composition) (11). This is especially important because breast tumors have higher magnesium (Mg) and

Submitted September 28, 2016, and accepted for publication December 16, 2016.

*Correspondence: aengler@ucsd.edu

Editor: Alissa Weaver.
http://dx.doi.org/10.1016/j.bpj.2016.12.038

calcium (Ca) concentrations than healthy breast tissue (18,19). Clinically, lower stromal cation concentrations have been associated with increasingly metastatic (20) and aggressive (21) tumors. As cancer cells migrate into the stroma, lower Mg^{2+} and Ca^{2+} concentrations may decrease integrin activation (22) and clustering (23,24), thus favoring the labile adhesions required for cancer cell migration (5). These data appear consistent with observations that integrin activation is inversely proportional to the metastatic potential of mammary cell lines (8), whereas traction forces are proportional (25). These data collectively suggest that heterogeneity in the adhesion-strength profile in stromal conditions may act as a biophysical marker, indicating the presence of a subset of metastatic cancer cells that are capable of disseminating into the stroma with lower Mg^{2+} and Ca^{2+} concentrations. Thus, we hypothesize that strongly adherent cells within a metastatic cell line will be the least migratory, and that adhesion strength is regulated by the sensitivity of assembled FAs to stromal Mg^{2+} and Ca^{2+} concentrations.

To understand how Mg^{2+} and Ca^{2+} influences cancer cell adhesion, we performed a spinning-disk analysis on epithelial and invasive cancer cell lines across a spectrum of metastatic potentials while varying the Mg^{2+} and Ca^{2+} levels. We observed a remarkable cellular heterogeneity and a decrease in cellular adhesion strength during the spinning-disk analysis. This was quantified by a decrease in logarithmic slope and a leftward shift in the τ_{25} value when shear stress was plotted versus cell density. This phenotype was only present in low Mg^{2+} and Ca^{2+} conditions for metastatic cell lines. These observations correlated with FA disassembly and were recapitulated in nonmetastatic cell lines that had been transformed to mirror their metastatic counterparts. The data further establish that metastatic cells with less labile adhesions and higher adhesion strength have reduced migration in collagen gels and transwell assays. These behaviors were independent of tumor and tissue type, and were demonstrated isogenically. These results support the concept that adhesion strength may act as a universal biophysical regulator of metastasis.

MATERIALS AND METHODS

Cell culture

Cells were cultured in their respective media as indicated in Table S1 in the Supporting Material, using typical formulations from Life Technologies (Carlsbad, CA) and the American Type Culture Collection (ATCC, Manassas, VA). When applicable, cells were selectively cultured with RGD peptides (Sigma, St. Louis, MO). All cells were cultured at 37°C in a humidified incubator containing 5% CO_2. Unless otherwise noted, cell culture products were purchased from Life Technologies. All cells were obtained from the ATCC cell bank and verified to be mycoplasma free. Cells were also authenticated by the ATCC based on morphology, growth curve analysis, and isoenzyme analysis, and were passaged for <6 months after resuscitation.

Cell adhesion-strength assay

Glass coverslips (25 mm, Fisher Scientific, St. Louis, MO) were sonicated in ethanol and pure water before incubation with 10 μg/mL human fibronectin (isolated from serum (26)) for 60 min at room temperature. All adhesion-strength assays were performed on fibronectin-coated coverslips unless otherwise noted, and 20 μg/mL type I collagen (rat tail; BD Biosciences, Franklin Lakes, NJ) was used. Under regular conditions, cells were allowed to attach for 24 h at 37°C and 5% CO_2 using cation-containing media. The coverslips were then mounted on a custom-built spinning-disk device and dipped into temperature-controlled spinning buffer (37°C) (11). Phosphate-buffered saline (PBS; without magnesium and calcium or with 0.5 mM $MgCl_2$ and 1 mM $CaCl_2$ (Cellgro, Manassas, VA)) was used as the spinning buffer. All spinning buffers contained 4.5 mg/mL dextrose. Once immersed in the spinning buffer, the coverslips were spun for 5 min at defined angular velocities and then the culture was continued or the cells were fixed with 3.7% formaldehyde immediately after spinning.

To select for strongly attaching cells, the center of the coverslips was covered with Parafilm that had been circularly cut with a crafting punch (The Punch Bunch, Temple, TX) and removed before shear application to ensure that all cells were subjected to a minimum shear. After 5 min of shear application, cells were allowed to recover in cell culture media for 1–2 h. The remaining cells were then trypsinized and replated on regular petri dish plastic. Control cells were treated likewise but without application of shear (i.e., 0 rpm).

Quantification of adhesion strength

Shear stress, τ, by radial fluid motion over the surface of the coverslip was calculated (10,27) such that:

$$\tau = \frac{4}{5} r \sqrt{\rho \mu \omega^3}, \quad (1)$$

where r is the radial position from the center of the disk, ρ is the buffer density, μ is the buffer viscosity, and ω is the rotational speed. To obtain quantitative information about the adhesion strength, whole 25 mm coverslips were imaged at 10× magnification on a Nikon (Melville, NY) Ti-S microscope (~1000 individual images stitched together with Metamorph 7.6 software and custom macros) and analyzed using a custom-written MATLAB (The MathWorks, Natick, MA) program. In brief, in this approach, the user defines the outer circle of the coverslip from a stitched overview image and the software then finds the position of each nucleus relative to the center of the coverslip. Cell densities, as a function of radial position and subsequently shear, are stored and combined with other measurements, e.g., those obtained at different RPMs. A sigmoidal decay fit is used to quantify values of adhesion strength and the logarithmic slope, i.e., the fit parameter in the sigmoid for curve steepness.

Migration assays

For two-dimensional migration experiments, tissue-culture-treated 12- and 24-well plates were coated with soluble rat-tail type I collagen in acetic acid (BD Biosciences) to achieve a coverage of 20 $\mu g/cm^2$ and incubated at room temperature for 1 h. For two-dimensional migration, collagen matrices at 1.2 and 2.4 mg/mL concentrations were prepared as described elsewhere (28). In brief, collagen was mixed with ice-cold PBS and 1 M NaOH was then added to normalize the pH to 7.0. Cells were imaged with a Nikon Eclipse Ti-S microscope equipped with a motorized temperature- and CO_2-controlled stage. Cells were imaged at 10× in bright field at multiple positions every 15 min for up to 48 h. Most of the migration data were analyzed by Time Lapse Analyzer, a freely available MATLAB program for cell migration analysis (29). Samples that could not be analyzed by the automated software (due to gel swelling and/or z-migration of the cells) were tracked manually with ImageJ (NIH, Bethesda, MD).

Additional migration experiments utilized six-well plates with transwell permeable supports (8 μm polycarbonate membrane; Corning, Corning, NY) that were seeded with 100,000 cells. After cells adhered to the permeable support, media was added to the whole well. Cells were allowed to migrate through the membrane for 24 h and then fixed and stained for nuclei (DAPI). Cells that successfully migrated through the membrane were counted on the bottom of the permeable support (ceiling). Additionally, cells that dropped off the support and adhered to the bottom of the six-well plate were also counted (bottom).

Immunofluorescence staining and focal adhesion analysis

Fixed cells were incubated for 10 min with 0.25% Triton X-100 followed by 1% albumin overnight at 4°C for blocking. Primary paxillin antibody (1:2000; ab32084, Abcam, Cambridge, UK) was applied for 2 h at room temperature. Then, a secondary Alexa Fluor 488-conjugated antibody (1:2000, Invitrogen, Carlsbad, CA) was applied for 1 h or rhodamine phalloidin (1:2000, Invitrogen) and Hoechst 33342 (3.2 μM, Invitrogen) were applied for 30 min at room temperature. The cells were subsequently mounted with Fluoromount-G (Southern Biotech, Birmingham, AL). All buffers contained 1 mM $MgCl_2$. The samples were imaged with the use of a CARV II confocal (BD Biosciences) Nikon Eclipse Ti-S microscope equipped with a motorized, programmable stage using a Cool-Snap HQ camera (Photometrics, Tucson, AZ) and controlled by Metamorph 7.6 (Molecular Devices, Sunnyvale, CA). A custom-written MATLAB program was used to quantify cell area and FA number and size (11). All FA metrics were computed across the entire cell to avoid regional biases.

Western blotting

Cell lysates were collected in mRIPA buffer (50 mM HEPES (pH 7.5), 150 mM NaCl, 1.5 mM $MgCl_2$, 1% Triton X-100, 1% Na-DOC, and 0.1% SDS) with 1 mM EGTA, 1 mM Na_3VO_4, 10 mM $Na_4P_2O_7$, and 1 mM phenylmethanesulfonylfluoride for Western blots. Samples were run in 10% SDS-PAGE gels at 150 V until proteins were separated and then transferred onto polyvinylidene fluoride membranes (Bio-Rad, Hercules, CA) to be run at 100 V for 1 h 15 min in the transfer apparatus (Bio-Rad). The membranes were washed in buffer A (25 mM Tris-HCl, 150 mM NaCl, and 0.1% Tween-20) 5% bovine serum albumin overnight at 4°C and then incubated for 2 h with the following antibodies: FA kinase (FAK; ab40794) at 1/500 and pFAK anti-phospho Y397 (ab4803) at 1/500 (both from Abcam), and glyceraldehyde 3-phosphate dehydrogenase (GAPDH; MAB374) at 1/250 (Millipore, Billerica, MA). After three 10-min washes with buffer A, secondary goat anti-rabbit horseradish peroxidase (Bio-Rad) and anti-mouse horseradish peroxidase (Abcam) were used for incubation for 30 min. Immunoblots were visualized using enhanced chemiluminescence reagent (Thermo Fisher, Waltham, MA).

Fluorescence-activated cell sorting analysis

Cells were detached from fibronectin-treated coverslips by incubation for 5–10 min with PBS without cations at 37°C and gentle pipetting. After resuspension in flow-cytometry buffer (DPBS, 2.5% goat serum, 1 mM EDTA (pH 7.4)), the cells were incubated with fluorescent-conjugated antibodies against CD49e (phycoerythrin) and CD51 (fluorescein isothiocyanate) (Biolegend, San Diego, CA) for 30 min on ice. Cells were analyzed using a FACScan flow cytometer (BD Biosciences).

Statistical analysis

Nonparametric Kruskal-Wallis analysis of variance tests were used for all statistical analyses unless indicated otherwise. All data in shear plots are expressed as mean ± SD. All experiments were performed at least in biological triplicate, and analyses represent hundreds of cells per condition.

RESULTS

Mg^{2+} and Ca^{2+} concentrations influence the adhesion heterogeneity of metastatic cells

To disseminate from primary tumors, metastatic cancer cells must invade adjacent stroma, which requires a transition from stable to labile adhesion. Using a spinning-disk device (Fig. S1), we measured the adhesion strength, τ_{25}, of mammary epithelial cell lines of varying metastatic potential. At physiological (serum) cation concentrations, i.e., 0.5 mM Mg^{2+} and 1 mM Ca^{2+} (denoted as PBS+MgCa), the adhesion strengths of nontumorigenic MCF10A cells, tumorigenic but not metastatic MCF7 cells, and tumorigenic and metastatic MDAMB231 cells to fibronectin were very similar, with no dramatic differences (Fig. 1, *black*). Mg^{2+} and Ca^{2+} concentrations differ between a healthy niche and tumor niche (18,19), and their removal during 5 min of shear application only slightly reduced the adhesion strength of MCF10A and MCF7 cells. However, the removal of Mg^{2+} and Ca^{2+} significantly reduced MDAMB231 cell adhesion strength (Fig. 1, *red*) by more than an order of magnitude (Fig. 1 *E*). Notably, the cell adhesion strength of the latter metastatic cell line was very heterogeneously distributed, with a significantly lower logarithmic slope versus nonmetastatic lines (Fig. 1 *F*). Given the significant genetic differences between these lines, we also assessed the adhesion strength of H-Ras-transformed MCF10A cells (labeled MCF10AT cells), which give rise to invasive carcinoma in vivo (30). As was the case with MDAMB231 cells, the MCF10AT cells showed Mg^{2+} and Ca^{2+} sensitivity, with lower τ_{25} and slightly more heterogeneity than MCF10A cells (Fig. 1 *D*, *open versus closed data points*). In contrast to fibroblasts (11), shear forces in the presence of Mg^{2+} and Ca^{2+} did not induce large changes in size for any of the cell lines tested. Furthermore, in the presence of Mg^{2+} and Ca^{2+}, variation in cell size across different cell lines was within the same order of magnitude. In these analyses, we visually assessed the cells to ensure that they were sufficiently spaced apart to prevent cell-cell interactions from disrupting the shear analysis (Fig. S2).

Although these data were obtained over a wide range of Mg^{2+} and Ca^{2+} concentrations, concentration gradients likely exist between the tumor and adjacent stroma (18,19). We found that homogeneous and strong adhesion strengths for metastatic cells, i.e., high τ_{25} and a logarithmic fit slope in density versus shear plots, could be gradually restored with increasing cation concentrations (Fig. 2 *A*), independently of cation type (Mg or Ca), with significant sensitivity at tumor and adjacent stroma concentrations

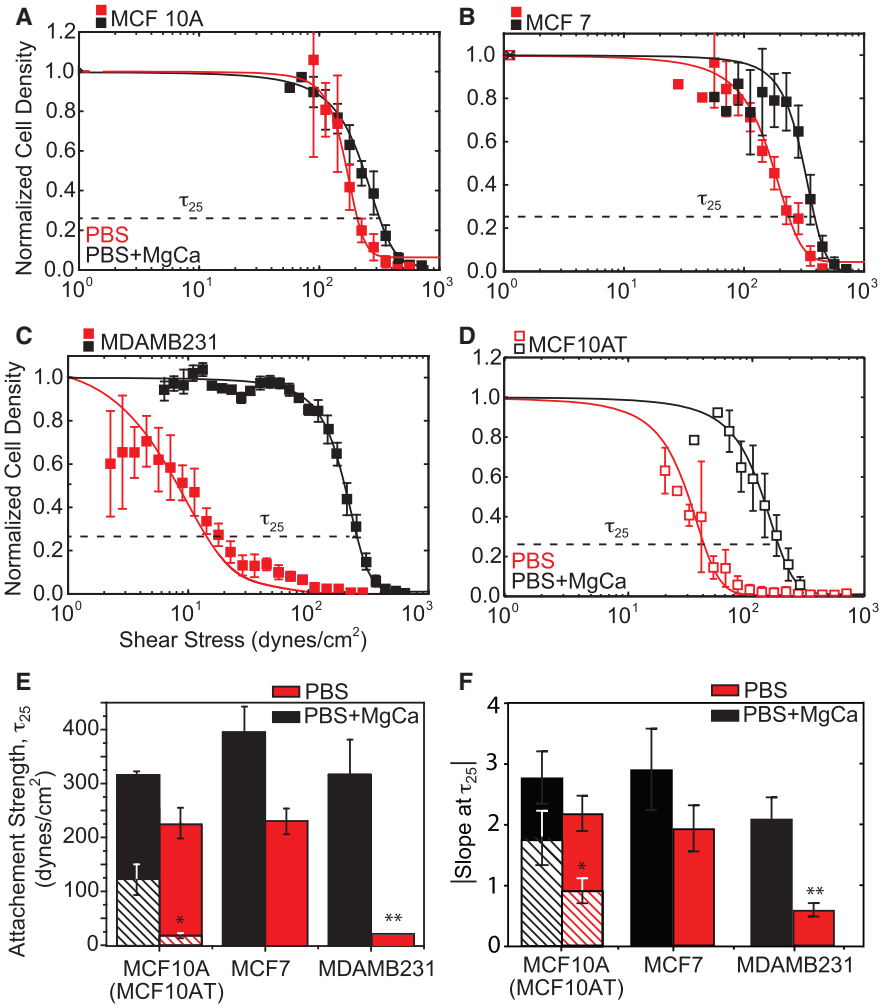

FIGURE 1 Adhesion strength is heterogeneous for metastatic mammary epithelial cells in a stromal-like niche. (*A–D*) Normalized cell density is plotted versus shear stress for (*A*) MCF10A (*closed*) and MCFA10T (*open*), (*B*) MCF7, (*C*) MDAMB231, and (*D*) MCF10AT cells. Shear stress was applied in buffer with (*black*) and without (*red*) 0.5 mM Mg^{2+} and 1 mM Ca^{2+}. τ_{25}, i.e., the shear to detach 25% of cells (also referred to as adhesion strength) is indicated in each plot. (*E*) Plot showing the average adhesion strength for cells exposed to shear in PBS buffer with (*black*) and without (*red*) cations. Crosshatched bars indicate data from MCF10AT cells. (*F*) Plot of the absolute magnitude of the logarithmic fit slope for each cell line and cation condition. All shear plots represent binned averages from biological triplicate experiments performed across multiple, overlapping shear ranges. All adhesion-strength assays were performed using fibronectin-coated coverslips. All other plots have $n > 3$. To see this figure in color, go online.

(Fig. 2 *B*). Mg^{2+}- and Ca^{2+}-dependent adhesion heterogeneity was also observed on type I collagen and could be gradually restored with increasing Mg^{2+} and Ca^{2+} concentrations (Fig. 2, *C* and *D*). Conversely, adhesion strength changes were minimal for nontumorigenic cells, which always exhibited strong adhesion (Fig. S3). Thus, metastatic mammary epithelial cells likely adhere in a metastatic-potential-dependent manner based on a subset of FA parameters.

Adhesive heterogeneity also extends beyond MDAMB231 cells to other metastatic cells. For comparison, we analyzed metastatic MDAMB468 and SUM1315 mammary cells by spinning-disk assay to determine the heterogeneity of their adhesion strength. The cells were sufficiently spaced apart to enable measurements of only the cell-matrix adhesion strength (27) (Fig. S2). Although it was not as robust as that observed for MDAMB231 cells, their adhesion strength was also heterogeneously distributed in terms of a lower τ_{25} and logarithmic fit slope, especially in comparison with BT20, an invasive but nonmetastatic mammary cell line, and BT549, a nonmalignant and nonmetastatic mammary cell line. PC-3 prostate carcinoma cells, a tumorigenic and highly metastatic cell line, also exhibited heterogeneously distributed adhesion (Fig. S4), indicating that common FA parameters may make adhesion strength a unique biophysical metric of cell state.

Adhesion heterogeneity correlates with a migratory phenotype

Although metastatic mammary epithelial cells display adhesive heterogeneity in a niche with low concentrations of Mg^{2+} and Ca^{2+}, it remains unclear how adhesion differences affect migration. We assessed cell migration in cell media containing physiological Mg^{2+} and Ca^{2+} concentrations first by selecting for strongly adherent cells, as outlined in Fig. 3 *A*. Migration appeared to change with relative adhesive heterogeneity in the absence of Mg^{2+} and Ca^{2+}; for example, minimal migration was observed for MCF10A cells and MDAMB231 cells selected with 45 dynes/cm^2 shear, whereas unselected MDAMB231 cells

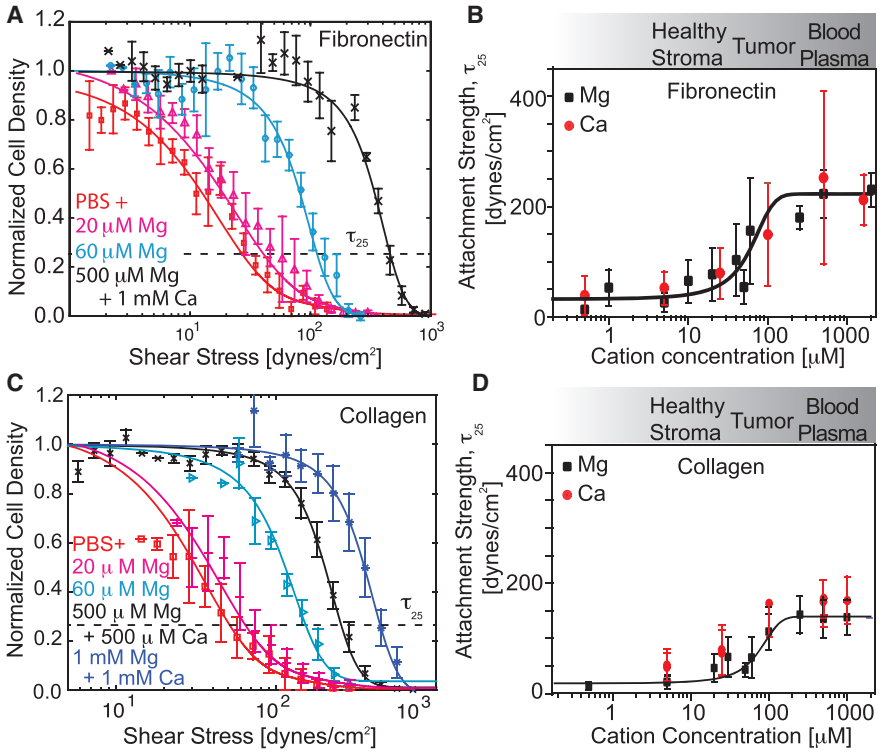

FIGURE 2 Adhesion strength can be titrated but is independent of the matrix ligand type. (*A*) Representative plot for MDAMB231 cells bound to fibronectin-coated coverslips versus the applied shear. Each color corresponds to the indicated cation condition; τ_{25} is indicated. (*B*) Plot of the average τ_{25} adhesion strength for MDAMB231 cells bound to fibronectin-coated coverslips versus cation concentration. The data are plotted separately for modulation of Mg^{2+} (*black squares*) or Ca^{2+} (*red circles*), but the sigmoidal fit is for the combined data. The cation concentration range for the indicated tissue is provided for reference based on Seltzer et al. (18,19). (*C*) Representative plot for MDAMB231 cells bound to collagen type I-coated coverslips versus the applied shear. Each color corresponds to the indicated cation condition; τ_{25} is indicated. (*D*) Plot of the average τ_{25} adhesion strength for MDAMB231 cells bound to collagen type I-coated coverslips versus cation concentration. The data are plotted separately for modulation of Mg^{2+} (*black squares*) or Ca^{2+} (*red circles*), but the sigmoidal fit is for the combined data. All shear plots represent binned averages from biological triplicate experiments performed across multiple, overlapping shear ranges. All other plots have $n > 3$. To see this figure in color, go online.

were significantly more motile (Fig. 3 *B*) and progressive in their migration. Migration of unselected MDAMB231 cells in collagen gels was increasingly persistent and linear with collagen concentration. Conversely, strongly adherent cells selected with high shear progressively lost their persistent, linear migration (Fig. 3 *C*). Other metastatic mammary cells, i.e., SUM1315, also demonstrated adhesive heterogeneity (Fig. S4), exhibiting more persistent, linear migration on collagen-coated, planar substrates than on collagen hydrogels. Migration of unselected SUM1315 cells, however, was more persistent and linear on collagen hydrogels compared with strongly adhering cells (Fig. S5 *A*). Migration of PC3 prostate cancer cells was also more persistent and linear with the unselected cell population (Fig. S5 *B*). These data suggest that shear selection can selectively isolate highly adhesive, Mg^{2+}- and Ca^{2+}-independent MDAMB231 cells, which appear to be less migratory than unselected MDAMB231 cells. Cell migration was also assessed using a transwell assay over 48 h. Relative to MCF10A cells, twice as many unselected MDAMB231 cells migrated through the pores. Metastatic cells demonstrating a strongly adherent phenotype during shear selection also exhibited decreased migration in the transwell assay. Interestingly, a significant number of MDAMB231 cells detached from the transwell insert and reattached to the chamber bottom. Significantly more MDAMB231 cells underwent this process compared with MCF10A (Fig. 3 *D*). Thus, the highly adhesive, Mg^{2+}- and Ca^{2+}-independent MDAMB231 cells appear to be less migratory than their unselected counterparts, which contain a highly migratory subpopulation.

Labile FAs reduce adhesion strength and enhance migration in metastatic cells

Although these data illustrate adhesive differences and their correlation to a migratory phenotype, they do not suggest an origin for these differences. Strongly adherent MDAMB231 cells did not differentially express integrins (Fig. 4 *A*), nor did phosphorylation of FAK change between MCF10A and MDAMB231 cells as a function of shear exposure (Fig. 4 *B*), suggesting a structural mechanism. Consistent with their adhesion strength, MCF10A cells did not fully disassemble their FAs (Fig. 4, *C* and *D*) and maintained their size and shape (Fig. 4, *E* and *F*) after Mg^{2+} and Ca^{2+} removal in the absence of shear. Conversely, metastatic MDAMB231 cells disassembled their FAs (Fig. 4, *G* and *H*) without significant changes in their size or morphology (Fig. 4, *I* and *J*). Thus, Mg^{2+} and Ca^{2+} sensitivity in the absence of shear suggests that MDAMB231 adhesions are transient and independent of the amount of elapsed culture time before shear application.

Although MCF10A cells did not exhibit Mg^{2+}- and Ca^{2+}-sensitive adhesion, we next asked whether we could induce FA disassembly and adhesion strength heterogeneity in these cells. Cells were seeded onto a fibronectin-coated substrate and pretreated with the fibronectin integrin-blocking peptide RGD. When the fibronectin-binding integrins were

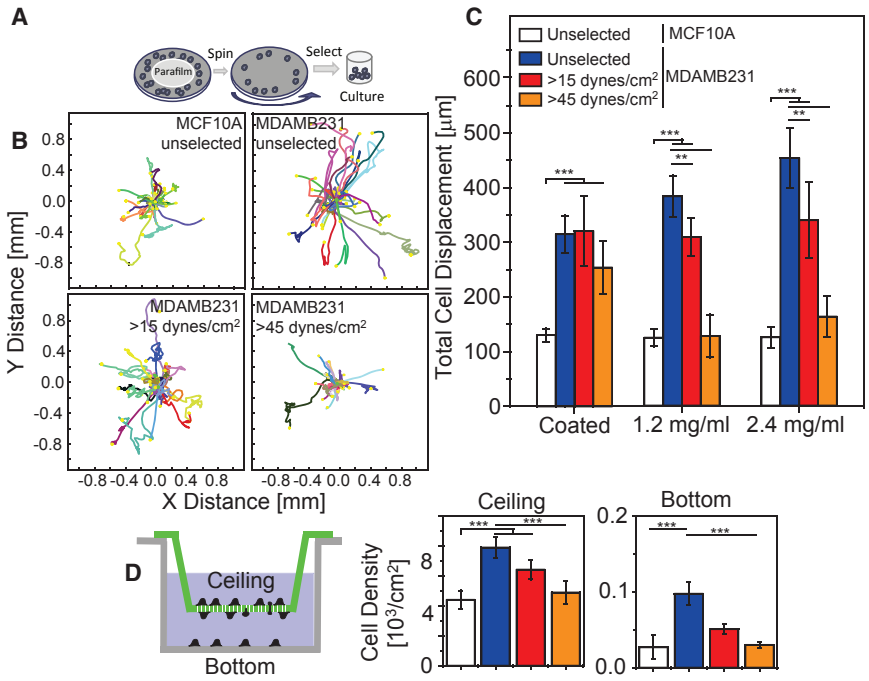

FIGURE 3 The weakly adherent subpopulation of MDAMB231 cells is highly migratory. (*A*) Schematic of the selection assay, where Parafilm is used to block the center of the coverslip so that cells only adhere to regions exposed to high shear stress. After trypsinization from collagen-coated coverslips, the cells are replated in migration or transwell assays. (*B*) Rose plots of cell migration trajectories for the indicated cell lines and shear stress selection conditions. Each trajectory represents an individual cell path on a collagen-coated substrate, as observed over 24 h. (*C*) Total cell displacement over 24 h for the indicated cell lines, shear stress selection conditions, and substrates. Each bar represents experiments performed in biological triplicate with >20 per sample and with each cell trajectory quantified at 15 min intervals over 24 h of imaging. (*D*) At left is an illustration of the transwell migration assay, indicating cells that have migrated through the pores of the membrane (*green*; referred to as the ceiling) and those cells that subsequently detached and reattached to the bottom of the well (*gray*). At right are graphs of cell density for the indicated cell lines and shear stress selection conditions. Cell densities on the ceiling of the insert (*top*) and bottom of the well (*bottom*) are shown separately and represent the results of triplicate biological replicates. $^{**}p < 0.01$, $^{***}p < 0.001$. To see this figure in color, go online.

blocked, cells without Mg^{2+} and Ca^{2+} exhibited statistically fewer FAs per area (Fig. 5, *A* and *B*). These data are consistent with fewer FAs but a different distribution from MDAMB231 cells (Fig. 5 *B* versus Fig. 4 *H*). When exposed to shear, RGD-treated MCF10A cells exhibited lower adhesion strengths but were not as heterogeneous as MDAMB231 cells (Fig. 5 *C*), possibly due to uniform integrin blocking with RGD ligand. Free RGD improved cell migration velocity (Fig. 5 *D*) to rates similar to those observed for MDAMB231 cells versus untreated nonmetastatic cells. Overall, these data suggest that FAs in metastatic cells are more Mg^{2+} and Ca^{2+} sensitive than those in nonmetastatic cells, and disassemble in stromal conditions (in contrast to nonmetastatic cells), thus driving the metastatic potential.

DISCUSSION

Cancer is a heterogeneous disease, which can be observed in comparisons between tumors, across cell lines, and even within a single cancer cell population. Complex tumor genotyping has been used to predict metastatic risk (31,32), and although these predictions are successful for some tumor subclasses (33), they do not identify the functional mediators of metastasis (34). Even in model cell lines, a subpopulation may develop increased metastatic potential under certain conditions that could inhibit metastasis for others. Rather than using biomarker(s) to predict metastatic potential (9), we tested a functional assay that allows the strength of cell adhesion to an underlying substrate to be observed ex vivo and in the appropriate context (i.e., with specific Mg^{2+} and Ca^{2+} concentrations to recapitulate tumor stroma) (18,19). It has been observed that lower cation concentrations, akin to those found in tumor stroma, create labile adhesions (5) and lead to increased metastasis (20) and invasion (21). We demonstrated that 1) a systematic quantification of metastatic versus nonmetastatic cells can reveal different adhesive phenotypes, and 2) that these differences are driven by changes in FA dynamics resulting from stromal niche conditions.

Cell-matrix adhesion is an exceedingly dynamic process (1). To capture that complexity in a context-specific manner, a systematic quantification of adhesion under appropriate tumor and stromal cation conditions is required. Classic wash assays involve cells adhering for a short period of time (<1 h), with subsequent rinsing steps to remove unbound cells (13). The undefined shear in such assays makes it difficult to quantitatively assess cancer cell adhesion. Although centrifugation and micropipette assays can impose a single shear amount per culture, they typically indicate that the number of bound cancer cells (14–16) and the amount of activated integrin (8) is inversely proportional to the metastatic potential of those cells. However, with the spinning-disk device, force is applied in a quantifiable and reproducible manner across the population (10). Furthermore, cation concentrations can also be probed directly since the cells remain in media (11). Under conditions that recapitulate estimated tumor Mg^{2+} and

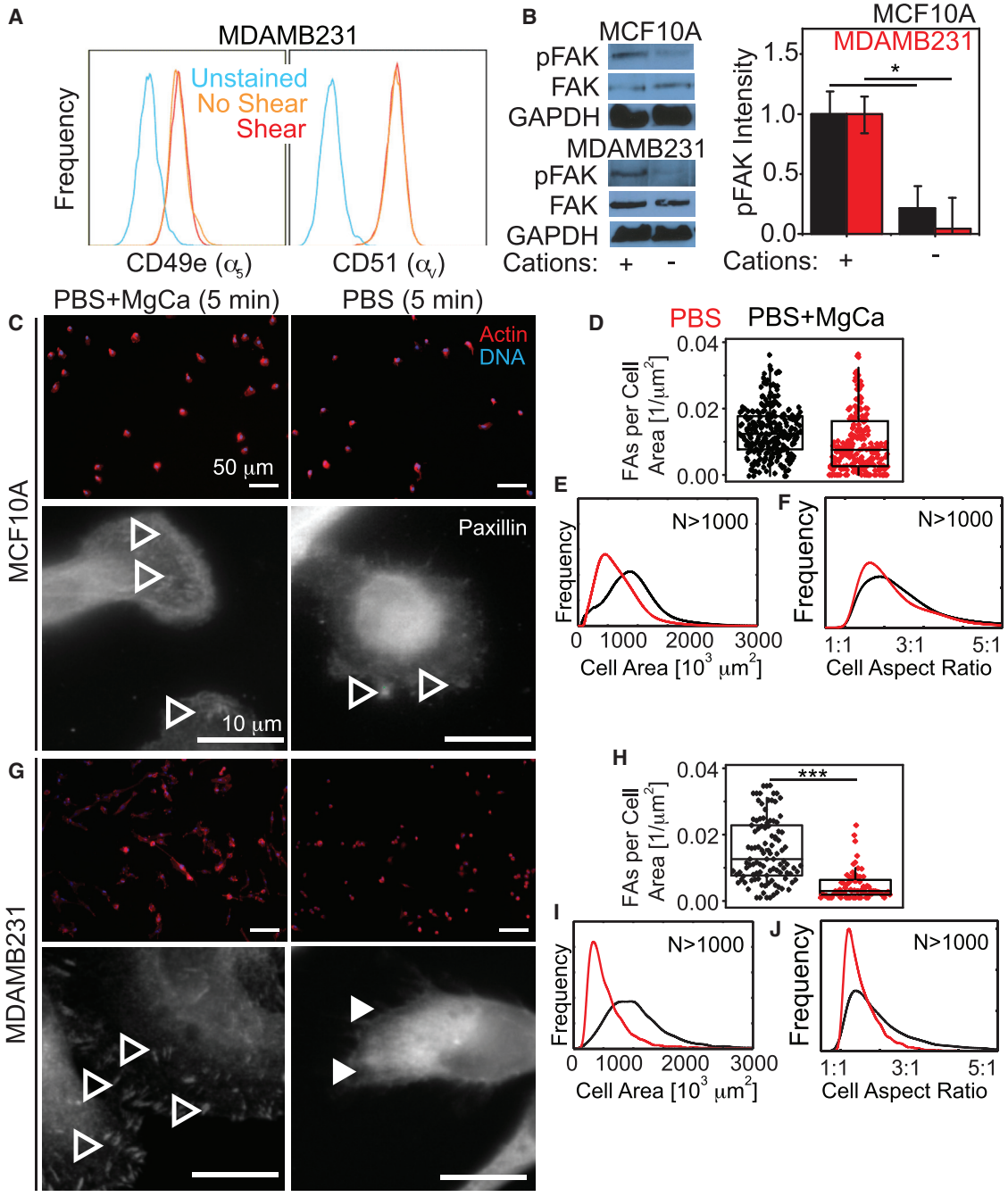

FIGURE 4 FAs are more Mg^{2+} and Ca^{2+} sensitive in MDAMB231 cells than in MCF10A cells. (*A*) Flow-cytometry profiles for the indicated integrins of MDAMB231 cells that were previously exposed (*red*) or not exposed (*orange*) to shear stress in the absence of cations. Unstained controls (*blue*) are shown for reference. (*B*) Representative Western blots for pFAK, total FAK, and GAPDH are shown for the indicated cells exposed to the indicated cation conditions for 5 min. Quantification of band intensity, normalized to GAPDH and total FAK, is shown for MCF10A and MDAMB231 cells with and without Mg^{2+} and Ca^{2+}. (*C*) Images of MCF10A cells in the indicated buffer conditions for 5 min without shear. Upper images are lower magnification and show cells stained for actin (*red*) and DNA (*blue*). Lower images are at higher magnification for the same conditions as the upper images and were stained for paxillin (*green*), actin (*red*), and DNA (*blue*). (*D*) Scatter plot of MCF10A cells, counting the number of FA plaques per square micron. (*E* and *F*) Frequency plots of MCF10A cell area and aspect ratio. (*G*) Images of MDAMB231 cells in the same conditions indicated in (*C*) for MCF10A cells. Open and closed arrowheads in (*C*) and (*G*) indicate cells with and without visible FAs, respectively. (*H*) Scatter plot of MDAMB231 cells, counting the number of FA plaques per square micron. (*I* and *J*) Frequency plots of MDAMB231 cell area and aspect ratio. In (*D–F*) and (*H–J*), cells incubated with and without cations for 5 min before measurement are shown in black and red, respectively. The scale bar represents 50 μm for all images. All adhesion assays were performed with fibronectin-coated coverslips. ***$p < 0.001$. All frequency and dot plots represent triplicate experiments analyzing 500+ cells per condition. To see this figure in color, go online.

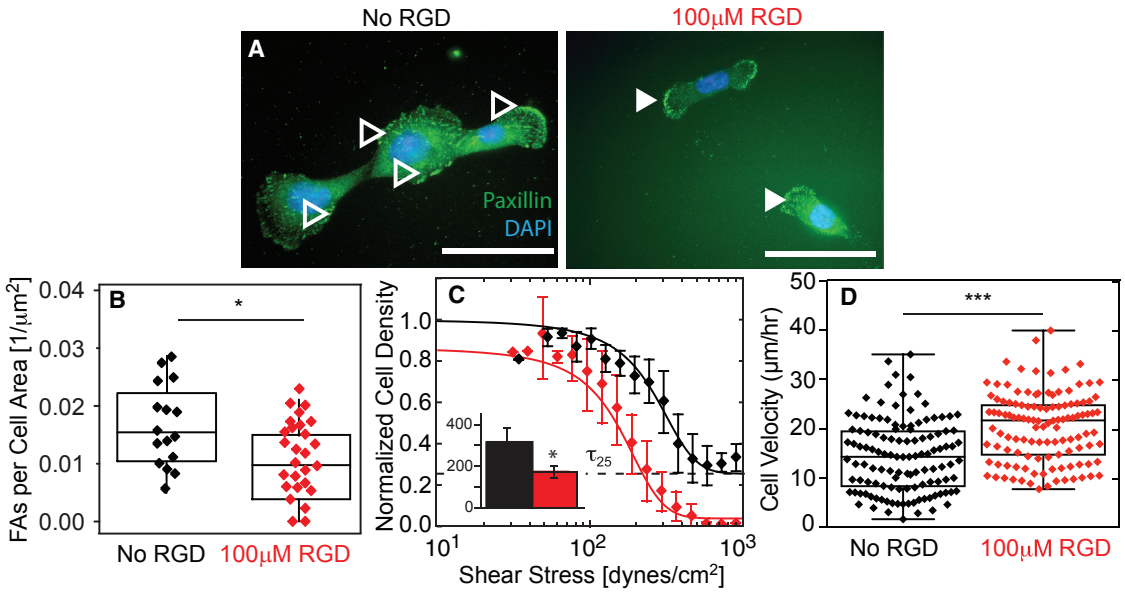

FIGURE 5 Integrin blocking reduces cation-dependent adhesion strength in nonmalignant cells. (*A*) MCF10A cells were stained for paxillin (*green*) and nuclei (*blue*). Open and closed arrowheads indicate FAs for the indicated RGD culture condition. Scale bars, 100 μm. (*B*) Plot of the number of FAs per cell area for cells without (*black*) and with (*red*) RGD. (*C*) Normalized cell density is plotted versus shear stress for cells without (*black*) and with (*red*) RGD. The inset shows the average τ_{25} adhesion strength for each condition in dynes per square centimeter. $*p < 0.05$. All dot plots represent triplicate experiments analyzing >20 cells per condition. Shear plots represent binned averages from biological triplicate experiments performed across multiple, overlapping shear ranges. All adhesion-strength assays were performed using fibronectin-coated coverslips. (*D*) Plot of cell velocity, in micrometers per hour, for cells treated (*red*) or not treated (*black*) with RGD on fibronectin-coated coverslips. $***p < 0.001$ for comparisons with unpaired *t*-test with Welch's correction. To see this figure in color, go online.

Ca^{2+} concentrations, e.g., 0.1–0.5 mM (18,19), we found that several mammary cell lines had adhesion strengths between 300 and 400 dynes/cm^2, regardless of the metastatic potential. At lower stromal cation concentrations, metastatic cells became significantly weaker and displayed adhesive heterogeneity, whether they originated from mammary (MDAMB231, SUM1315, and MDAMB468) or prostate (PC3) cancers. In contrast, nonmetastatic cell lines did not demonstrate significant adhesion strength heterogeneity. Moreover H-Ras transformation of a nonmetastatic cell line caused it to adopt adhesive heterogeneity only in Mg^{2+}- and Ca^{2+}-free conditions, indicating that independently of their genetic background, metastatic cell lines vary significantly in adhesion strength. Together with previous findings (14–16), these data establish an adhesion dependence on stromal-like conditions for a subset of metastatic cells.

The mechanism(s) behind adhesive heterogeneity and cation sensitivity in cells appears to be complex, whether the cells are selected by shear or not. Although metastatic behavior was previously linked to diminished integrin activation (8), we found no change in integrin expression or FAK phosphorylation that was independent of the buffer conditions used. However, blocking ion channels in metastatic mammary and prostate cancer cells artificially enhanced their adhesion in single-cell assays versus control cells (14), suggesting that cation effects are plausible. Indeed, we found that MCF10A adhesions were less cation sensitive than MDAMB231 adhesions, as their FA size and number changed less after Mg^{2+} and Ca^{2+} removal in comparison with the MDAMB231 cells. Similarly, when MCF10A cell FA assembly was modulated by the addition of soluble RGD, the resulting changes in FAs reduced adhesion strength in a manner consistent with that observed for MDAMB231 cells. It should be noted that MCF10A cells were more sensitive to ligand type, although the sensitivity was always observed with adhesion strengths well above 100 dynes/cm^2. The sensitivity of MDAMB231 cells was observed at lower adhesion strengths and also induced heterogeneous adhesion, i.e., a shallow logarithmic slope. Under comparable matrix and cation conditions, MCF10A cells never exhibited heterogeneous adhesion. Together, these data suggest that assembly differences in low Mg^{2+} and Ca^{2+} conditions in the stroma could drive adhesion strength heterogeneity. As such, assembly changes have been equated to differences in turnover (7) and might be expected to create MDAMB231 cells with labile adhesions required for 3D protrusion and migration (28). This interpretation is consistent with metastatic and invasive behaviors observed in low Mg^{2+}- and Ca^{2+}-containing stroma (20,21). We also showed that shear selection of the strongly adhering subpopulation of MDAMB231 cells (>45 dynes/cm^2) suppressed their migration on collagen gels and their ability to migrate through transwells, such that they resembled the less cation-sensitive, nonmetastatic cells. Although the origin of increased FA cation sensitivity

remains unclear, the mechanism is not specific to mammary cells, since adhesion-selected PC3 prostate cancer cells also failed to migrate on substrates and/or in transwell assays as did their unselected counterparts. Together, these data suggest that there is a common heterogeneous adhesive signature in cell lines described as having metastatic potential, and importantly, within this population is a subset of weakly adherent, highly migratory cells.

CONCLUSIONS

Given the heterogeneity and plasticity observed in the adhesive phenotype and the inverse correlation between migration and strongly adherent subpopulations, the data presented here emphasize the importance of therapeutically targeting as many cancer cell states as possible, instead of focusing on the largest population or most aggressive phenotypes. These data also suggest that the adhesive state, when measured in the appropriate stromal cation concentrations, could serve as a unique biophysical marker for highly migratory behavior in metastatic cells generally.

SUPPORTING MATERIAL

Five figures and one table are available at http://www.biophysj.org/biophysj/supplemental/S0006-3495(17)30029-2.

AUTHOR CONTRIBUTIONS

Conceptualization: A.F. and A.J.E. Methodology: A.F., A.B., and T.D.T. Investigation: A.F., A.B., and P.B. Writing: A.F., T.D.T., and A.J.E. Review and editing: A.F., A.B., P.B., T.D.T., and A.J.E. Funding acquisition: A.B. and A.J.E. Supervision: A.J.E.

ACKNOWLEDGMENTS

The authors thank Drs. Caroline Damsky and David Strom for antibodies obtained via the Developmental Studies Hybridoma Bank under the auspices of the National Institute of Child Health and Human Development, and maintained by the University of Iowa (Iowa City, IA). The authors also thank Dr. Philippe Gascard for a helpful review of the manuscript. The spinning-disk device was designed and manufactured by Jeremy Riley, Ryan Tam, Joe Shu, and the UC San Diego Campus Research Machine Shop.

This work was supported by grants from the National Institutes of Health (DP2OD006460 and U54CA143803-03 to A.J.E.), the Department of Defense (W81XWH-13-1-0133 to A.J.E.), and the National Science Foundation Graduate Research Fellowship Program (to A.B. and P.B.).

REFERENCES

1. Wirtz, D., K. Konstantopoulos, and P. C. Searson. 2011. The physics of cancer: the role of physical interactions and mechanical forces in metastasis. *Nat. Rev. Cancer.* 11:512–522.
2. Quintana, E., M. Shackleton, …, S. J. Morrison. 2008. Efficient tumour formation by single human melanoma cells. *Nature.* 456:593–598.
3. Levental, K. R., H. Yu, …, V. M. Weaver. 2009. Matrix crosslinking forces tumor progression by enhancing integrin signaling. *Cell.* 139:891–906.
4. Paszek, M. J., N. Zahir, …, V. M. Weaver. 2005. Tensional homeostasis and the malignant phenotype. *Cancer Cell.* 8:241–254.
5. Zaman, M. H., L. M. Trapani, …, P. Matsudaira. 2006. Migration of tumor cells in 3D matrices is governed by matrix stiffness along with cell-matrix adhesion and proteolysis. *Proc. Natl. Acad. Sci. USA.* 103:10889–10894.
6. Ridley, A. J., M. A. Schwartz, …, A. R. Horwitz. 2003. Cell migration: integrating signals from front to back. *Science.* 302:1704–1709.
7. Bijian, K., C. Lougheed, …, M. A. Alaoui-Jamali. 2013. Targeting focal adhesion turnover in invasive breast cancer cells by the purine derivative reversine. *Br. J. Cancer.* 109:2810–2818.
8. Indra, I., V. Undyala, …, K. A. Beningo. 2011. An in vitro correlation of mechanical forces and metastatic capacity. *Phys. Biol.* 8:015015.
9. Liu, Y., R. Nenutil, …, P. J. Coates. 2014. Lack of correlation of stem cell markers in breast cancer stem cells. *Br. J. Cancer.* 110:2063–2071.
10. Boettiger, D. 2007. Quantitative measurements of integrin-mediated adhesion to extracellular matrix. *Methods Enzymol.* 426:1–25.
11. Fuhrmann, A., J. Li, …, A. J. Engler. 2014. Cation type specific cell remodeling regulates attachment strength. *PLoS One.* 9:e102424.
12. Gallant, N. D., and A. J. García. 2007. Model of integrin-mediated cell adhesion strengthening. *J. Biomech.* 40:1301–1309.
13. Yates, C. M., H. M. McGettrick, …, G. E. Rainger. 2014. Adhesion of tumor cells to matrices and endothelium. *Methods Mol. Biol.* 1070:57–75.
14. Palmer, C. P., M. E. Mycielska, …, M. B. Djamgoz. 2008. Single cell adhesion measuring apparatus (SCAMA): application to cancer cell lines of different metastatic potential and voltage-gated Na+ channel expression. *Eur. Biophys. J.* 37:359–368.
15. Reticker-Flynn, N. E., D. F. Malta, …, S. N. Bhatia. 2012. A combinatorial extracellular matrix platform identifies cell-extracellular matrix interactions that correlate with metastasis. *Nat. Commun.* 3:1122.
16. Fischer, E. G., M. Riewald, …, W. Ruf. 1999. Tumor cell adhesion and migration supported by interaction of a receptor-protease complex with its inhibitor. *J. Clin. Invest.* 104:1213–1221.
17. Gupta, P. B., C. M. Fillmore, …, E. S. Lander. 2011. Stochastic state transitions give rise to phenotypic equilibrium in populations of cancer cells. *Cell.* 146:633–644.
18. Seltzer, M. H., F. E. Rosato, and M. J. Fletcher. 1970. Serum and tissue magnesium levels in human breast carcinoma. *J. Surg. Res.* 10: 159–162.
19. Seltzer, M. H., F. E. Rosato, and M. J. Fletcher. 1970. Serum and tissue calcium in human breast carcinoma. *Cancer Res.* 30:615–616.
20. Nasulewicz, A., J. Wietrzyk, …, A. Opolski. 2004. Magnesium deficiency inhibits primary tumor growth but favors metastasis in mice. *Biochim. Biophys. Acta.* 1739:26–32.
21. Dai, Q., S. S. Motley, …, J. H. Fowke. 2011. Blood magnesium, and the interaction with calcium, on the risk of high-grade prostate cancer. *PLoS One.* 6:e18237.
22. Mould, A. P., S. K. Akiyama, and M. J. Humphries. 1995. Regulation of integrin alpha 5 beta 1-fibronectin interactions by divalent cations. Evidence for distinct classes of binding sites for Mn2+, Mg2+, and Ca2+. *J. Biol. Chem.* 270:26270–26277.
23. Geiger, B., J. P. Spatz, and A. D. Bershadsky. 2009. Environmental sensing through focal adhesions. *Nat. Rev. Mol. Cell Biol.* 10:21–33.
24. Parsons, J. T., A. R. Horwitz, and M. A. Schwartz. 2010. Cell adhesion: integrating cytoskeletal dynamics and cellular tension. *Nat. Rev. Mol. Cell Biol.* 11:633–643.
25. Kraning-Rush, C. M., J. P. Califano, and C. A. Reinhart-King. 2012. Cellular traction stresses increase with increasing metastatic potential. *PLoS One.* 7:e32572.

26. Mao, Y., and J. E. Schwarzbauer. 2005. Stimulatory effects of a three-dimensional microenvironment on cell-mediated fibronectin fibrillogenesis. *J. Cell Sci.* 118:4427–4436.

27. Fuhrmann, A., and A. J. Engler. 2015. Acute shear stress direction dictates adherent cell remodeling and verifies shear profile of spinning disk assays. *Phys. Biol.* 12:016011.

28. Fraley, S. I., Y. Feng, …, D. Wirtz. 2010. A distinctive role for focal adhesion proteins in three-dimensional cell motility. *Nat. Cell Biol.* 12:598–604.

29. Huth, J., M. Buchholz, …, H. A. Kestler. 2011. TimeLapseAnalyzer: Multi-target analysis for live-cell imaging and time-lapse microscopy. *Comput. Methods Programs Biomed.* 104:227–234.

30. Heppner, G. H., and S. R. Wolman. 1999. MCF-10AT: a model for human breast cancer development. *Breast J.* 5:122–129.

31. van 't Veer, L. J., H. Dai, …, S. H. Friend. 2002. Gene expression profiling predicts clinical outcome of breast cancer. *Nature.* 415: 530–536.

32. Paik, S., S. Shak, …, N. Wolmark. 2004. A multigene assay to predict recurrence of tamoxifen-treated, node-negative breast cancer. *N. Engl. J. Med.* 351:2817–2826.

33. Subramaniam, D. S., and C. Isaacs. 2005. Utilizing prognostic and predictive factors in breast cancer. *Curr. Treat. Options Oncol.* 6: 147–159.

34. Valastyan, S., and R. A. Weinberg. 2011. Tumor metastasis: molecular insights and evolving paradigms. *Cell.* 147:275–292.

Biophysical Journal, Volume *112*

Supplemental Information

Metastatic State of Cancer Cells May Be Indicated by Adhesion Strength

Alexander Fuhrmann, Afsheen Banisadr, Pranjali Beri, Thea D. Tlsty, and Adam J. Engler

SUPPLEMENTAL FIGURES

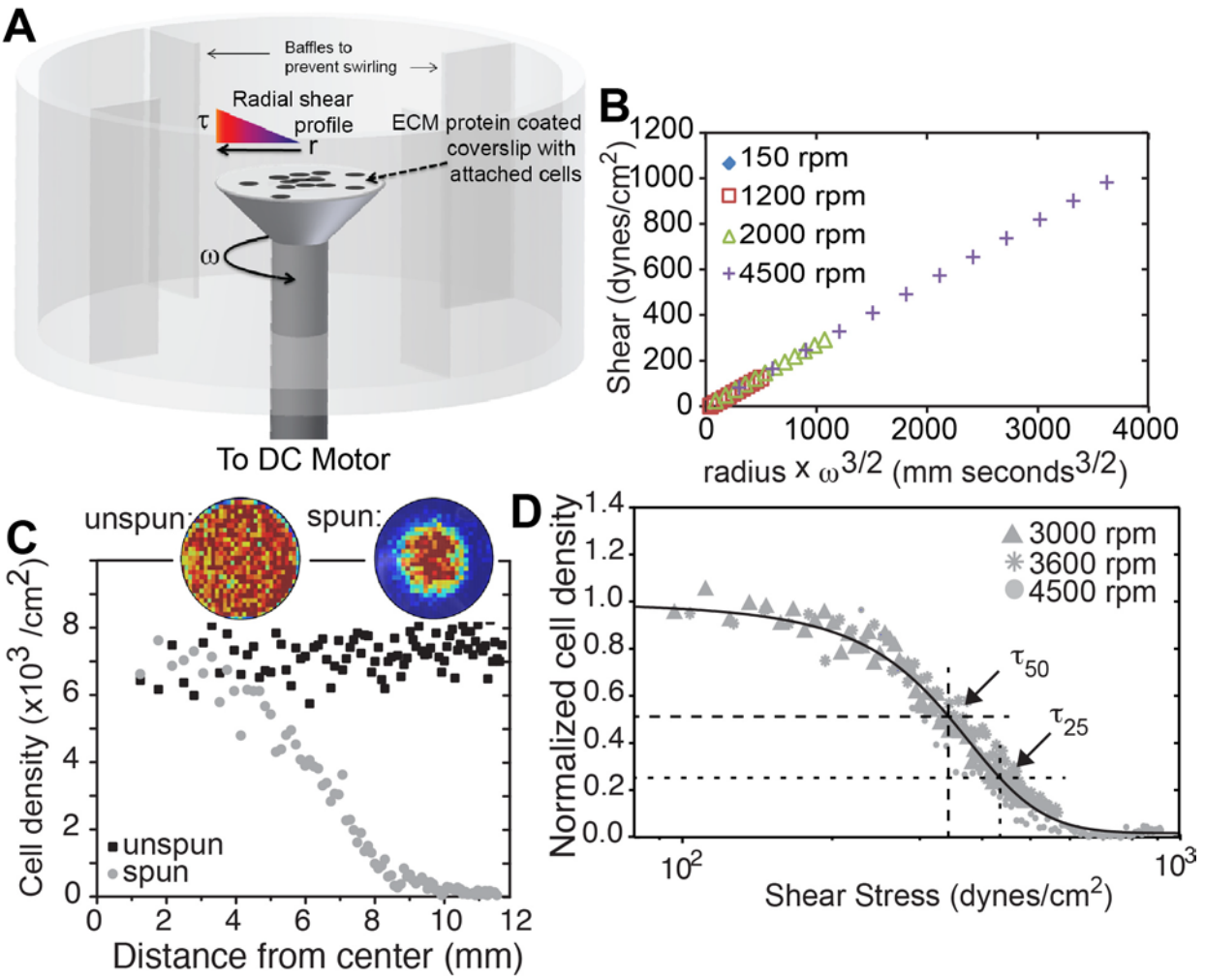

Figure S1: Spinning Disc Assay Creates a Radially-dependent Shear Profile. (A) The spinning disc device is illustrated with cells attached to an extracellular matrix protein-coated coverslip mounted and rotating on a spinning rod in buffer. The radially-dependent shear profile is highlighted showing that cells at the center only rotate in place while those at the edge move around at a high linear velocity. (B) The plot shows the relationship of radial position on the coverslip and angular velocity versus applied shear stress at a given point for the indicated velocities (in revolutions per minute; rpm). (C) Plot of the relationship between radial position and cell density. Inset images show heat maps of cell density. Warm (red) and cool (blue) colors indicate high and low densities, respectively. (D) Plot of cell density, normalized to the center of the coverslip, versus the applied shear. Data is plotted for the indicated velocities. τ_{25} and τ_{50}, i.e. the shear to detach 25 and 50% of cells, respectively, are indicated in the plot and are 438 and 346 dynes/cm^2, respectively.

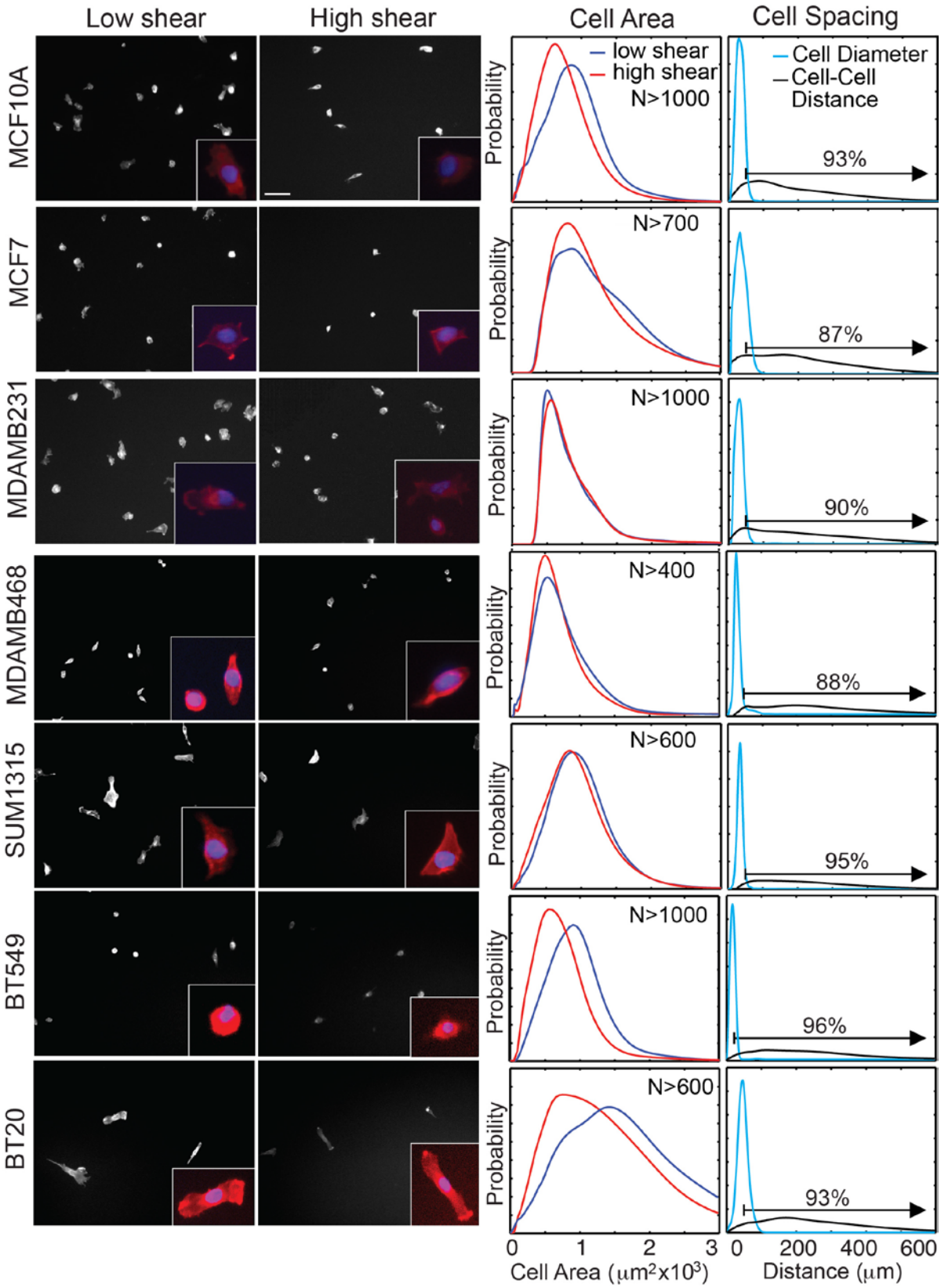

Figure S2: Cell Morphology and Distribution are Independent of Mammary Epithelial Cell Line. At the left are low magnification images of MCF10A, MCF7, MDAMB231, MDAMB468,

SUM1315, BT549, and BT20 cells at low and high shear, which were stained with Rhodamine-Phalloidin. Inset images at higher magnification were also stained with DAPI. At right are plots of cell area (blue and red lines indicating high and low shear) and cell-to-cell spacing frequency for the indicated number of cells (N). Indicated within the plots is the percentage of cells spaced further apart than the average diameter of each cell line.

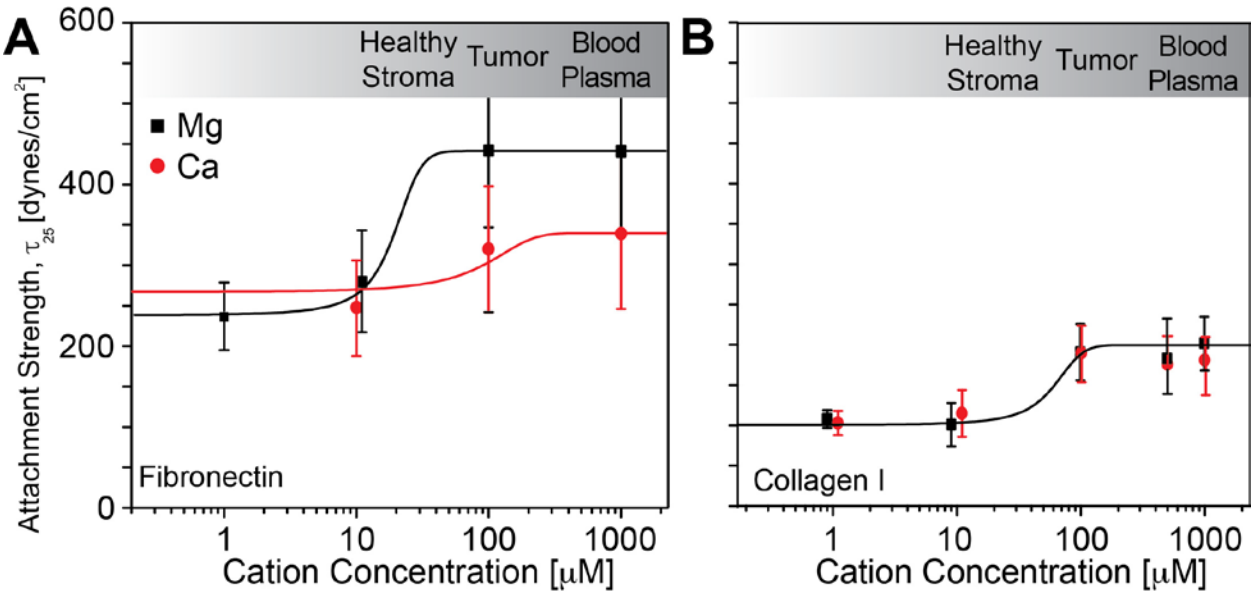

Figure S3: MCF10A Cells Exhibit Cation-Sensitive Change in Attachment Strength. For MCF10A, cells had homogeneous and strong attachment strengths, i.e. τ_{25}, as plotted versus cation concentration for Mg^{2+} (black squares) and Ca^{2+} (red circles) for cells bound to (A) collagen type I-coated and (B) fibronectin-bound coverslips. Cation concentration range for the indicated tissue is provided for reference. A sigmoidal fit for each cation is shown in panel A but they are combined in panel B.

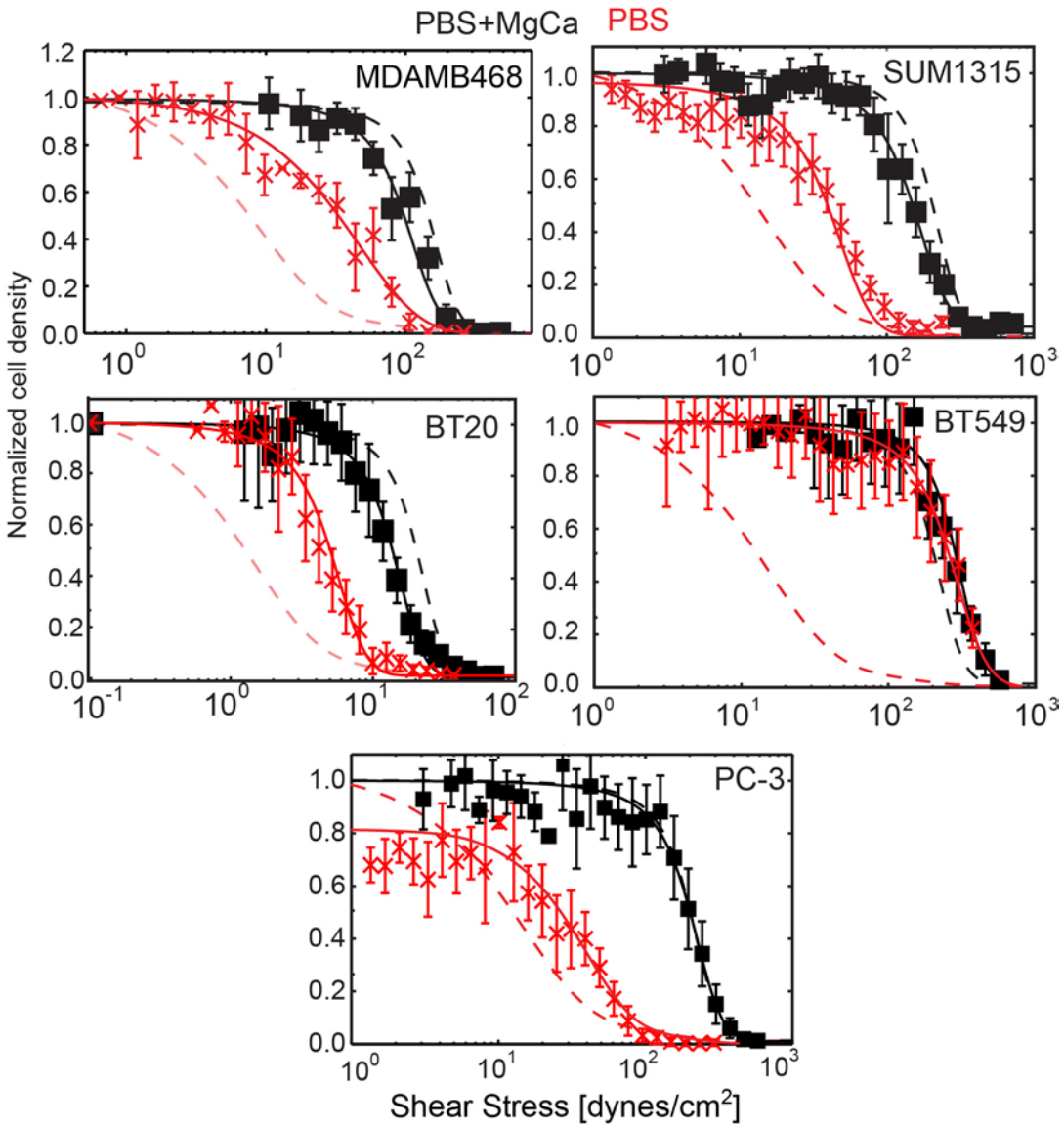

Figure S4: Attachment Strength is Heterogeneous for Additional Mammary Epithelial Cells and Prostate Cancer Cells in Stromal-like Niche. Normalized cell density is plotted versus shear for MDAMB468, SUM1315, BT20, BT549 and PC-3 cells. Cells were tested with (black) and without (red) media containing cations as defined in Figure 1. Dashed lines in each plot indicate the fits for MDAMB231 cells with (black) and without (red) media containing cations.

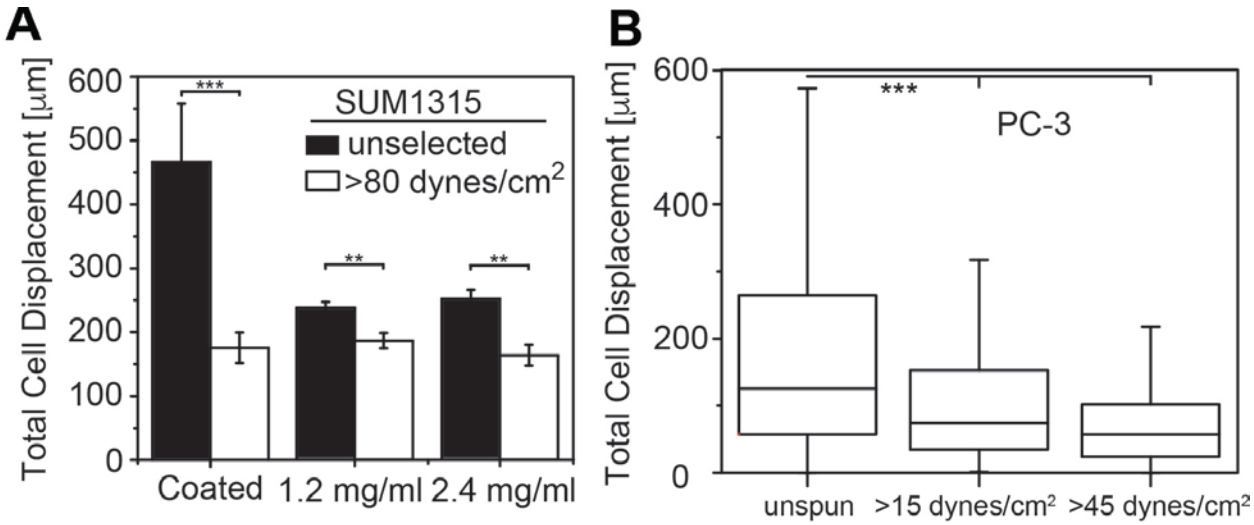

Figure S5: Migration for SUM1315 and PC-3. (A) SUM1315 cells, either unselected (blue) or selected with 80 dynes/cm^2 (orange), plated onto collagen-coated, planar substrates (left) and 1.2 mg/ml (center) and 2.4 mg/ml (right) collagen hydrogels were plotted for the total distance migrated over 24 hours post-plating. Note that the migration of many unselected cells on planar surfaces exceeded the viewable window of the microscope over 24 hours, and thus these data represent a minimum distance traveled. (B) Total cell displacement over 24 hours for PC3 cells are plotted for the indicated shear stress selection conditions on collagen-coated substrates. PC-3 cell migration is more heterogeneous and thus displayed in a box and whisker plot **p <0.01, ***p < 0.001.

SUPPLEMENTAL TABLE

Cell Line	Base Media	Serum	Antibiotics	Others
MCF10A, MCF10AT	DMEM/ F12	5% HS	100 units/ml Penicillin, 100 µg/ml Streptomycin	0.5 µg/ml Hydrocortisone, 20 ng/ml hEGF, 10 µg/ml Insulin, 100 ng/ml Cholera toxin
MCF7	DMEM	10% FBS	100 units/ml Penicillin, 100 µg/ml Streptomycin	10 µg/ml Insulin
MDAMB231, MDAMB468, BT20	DMEM	10% FBS	100 units/ml Penicillin, 100 µg/ml Streptomycin	
SUM1315	DMEM/ F12	5% FBS	100 units/ml Penicillin, 100 µg/ml Streptomycin	5µg/ml hEGF, 5 µg/ml Insulin
BT549	DMEM	10% FBS	100 units/ml Penicillin, 100 µg/ml Streptomycin	1 µg/ml Insulin
PC3	F-12K	10% FBS	100 units/ml Penicillin, 100 µg/ml Streptomycin	

Table S1: Media formulations for the indicated cell lines.